APPLICATIONS OF THE DISCRETE GREEN'S FUNCTION IN THE FINITE-DIFFERENCE TIME-DOMAIN METHOD

Tomasz P. Stefanski[*]

Department of Microwave and Antenna Engineering, Faculty of Electronics, Telecommunications and Informatics, Gdansk University of Technology, Gdansk 80-233, Poland

Abstract—In this paper, applications of the discrete Green's function (DGF) in the three-dimensional finite-difference time-domain (FDTD) method are presented. The FDTD method on disjoint domains was developed employing DGF to couple the FDTD domains as well as to compute the electromagnetic field outside these domains. Hence, source and scatterer are simulated in separate domains and updating of vacuum cells, being of little interest from a user point of view, can be avoided. In the developed method, the field radiated by an FDTD domain is computed as a convolution of DGF with equivalent current sources measured over two displaced Huygens surfaces. Therefore, the computed electromagnetic field is compatible with the FDTD grid and can be applied as an incident wave in a coupled total-field/scattered-field domain. In the developed method, the DGF waveforms are truncated using the Hann's window and windowing parameters assuring accuracy of computations are pointed out. The error of the field computations varies between $-90\,\text{dB}$ and $-40\,\text{dB}$ depending on the DGF length and excitation waveform. However, if the DGF length is equal to the number of iterations in a simulation, the presented DGF-based techniques return the same results as the direct FDTD method.

1. INTRODUCTION

Recently, the discrete Green's function (DGF) [1–4] has been proven to be an efficient tool facilitating the finite-difference time-domain (FDTD) method [5–11]. DGF is a response of the FDTD grid to the

---

Kronecker delta current source. It is directly derived from the FDTD update equations, thus the FDTD method and its integral discrete formulation based on DGF can be perfectly coupled [12]. Consequently, DGF has proven useful for FDTD simulations of antennas with savings in runtime and memory usage [12–15].

DGF incorporates numerical artifacts inherent in the use of the discrete computational domain, i.e., numerical dispersion, anisotropy and limitation of the time-step size due to the stability constraint. The continuous Green's function (CGF) does not exhibit these properties, thus its applicability in the FDTD method is questionable. The problem of mismatch between directly sampled continuous solutions of Maxwell's equations and the FDTD grid is vitally important for the total-field/scattered-field (TFSF) simulations [5]. For instance, non-physical reflections approaching 10% of an incident plane wave were reported when an analytic source was exciting the FDTD grid [16, 17]. Whereas injection of the plane wave into the FDTD grid was extensively studied in the literature, the problem of arbitrary excitation of the TFSF domain was rather marginally investigated. However, Schneider et al. [18] have already noticed that DGF can be employed to inject the field into the TFSF domain without any errors.

The field radiated from an FDTD domain can also be computed using CGF which is inconsistent with the electromagnetic theory on a grid [19–23]. FDTD simulations on disjoint domains [24, 25] are an example of application which requires DGF to couple FDTD domains. It is shown below that the application of CGF in the time-marching procedure of the FDTD method may lead to noncasual or inaccurate results.

The objective of this paper is to demonstrate the three-dimensional (3-D) DGF applications for coupling FDTD domains as well as for computing the electromagnetic field outside these domains. To the best of the author's knowledge, the coupling of FDTD domains with the use of DGF has only been presented in two dimensions up to now. In the presented method, the 3-D FDTD domains can be associated with simulated objects, whilst the interaction between them is modeled with the use of DGF. Therefore, the number of updated cells in the computational domain can be reduced and vacuum cells, being of little interest from a user point of view, can be excluded from the update procedure. Moreover, DGF allows to decompose an FDTD domain for execution of computations on distributed-memory parallel computing architectures. The proposed DGF applications are examined in several numerical tests showing accuracy of (i) the field radiated from an FDTD domain to a single observation point, (ii) unilateral coupling between FDTD domains and (iii) bilateral

coupling between FDTD domains with half-wavelength dipole antennas inside.

    This paper is organized as follows. The ideas of the FDTD method on disjoint domains and DGF computations are presented in Section 2. In Section 3, the drawbacks of the CGF application in the time-marching procedure of the FDTD method are demonstrated and discussed. In Section 4, the results of numerical tests are presented. Finally, the conclusions are given in Section 5.

2. DGF APPLICATIONS IN THE FDTD METHOD

The ideas behind the proposed DGF applications facilitating the FDTD method are presented in Fig. 1.   The radiated field computations (Fig. 1(a)) are necessary in the FDTD solver on disjoint domains because a user may occasionally want to inspect time-domain waveforms of the field outside these domains. Moreover, the radiated field computations replace the standard near-to-far field transformation [5] in the FDTD solver on disjoint domains. An extra advantage here is that the code of the radiated field computations can easily be extended in order to excite a coupled TFSF domain (see Fig. 1(b)). Hence, the unilateral coupling between weakly coupled FDTD domains can be simulated. Currently, commercial FDTD solvers allow running two-stage simulations with the source of radiation simulated at the first stage and multiple simulations of the irradiation at the second stage [26]. Hence, many different objects weakly coupled with the source of radiation can be simulated with savings in the runtime and memory usage [27]. The DGF propagator allows transferring the electromagnetic field to observation points outside the computational domain from cells in close proximity to the source of radiation. Therefore, the DGF-based computations of unilateral coupling between FDTD domains can also be applied to compute an incident wave for such two-stage FDTD simulations of irradiation. Extension of this algorithm towards a simulation of strongly coupled objects results in the FDTD method on disjoint domains [28]. In this method, the TFSF surfaces of excitations are placed inside the Huygens boxes and the interaction between domains is bilateral.

    In the computational techniques shown in Fig. 1, the source of radiation (e.g., antenna) and the scatterer are placed in separate FDTD domains terminated by the perfectly matched layers (PMLs). Although DGF can also provide a global absorbing boundary condition (ABC) in the FDTD method, computational efficiency of global ABCs is very low in comparison to PMLs. The developed techniques are consistent with the equivalence theorem in the discrete domain [29, 30].
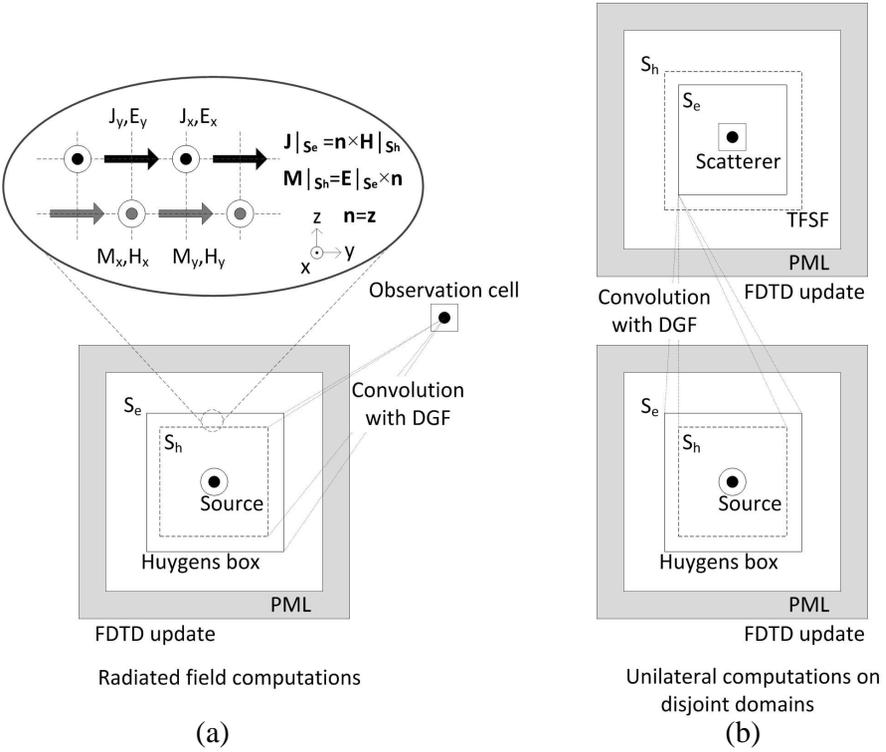
Figure 1. Implementations of (a) the radiated field computations for a single FDTD domain and (b) the FDTD method on disjoint domains with the unilateral coupling.

Each Huygens box comprises of two surfaces, separated by a half-cell distance, placed in close proximity to the simulated object. Outer and inner surfaces of the Huygens box respectively correspond to the electric and magnetic equivalent current sources (refer to Fig. 1(a)). In the FDTD method on disjoint domains with bilateral coupling, the inner surface of the Huygens box is also a part of the TFSF box [28].

The electromagnetic field is computed outside a radiating domain as a convolution of current sources $\mathbf{J}$, $\mathbf{M}$ and dyadic DGF [12]:

$$\begin{bmatrix} \mathbf{E}|_{ijk}^n \\ \eta\mathbf{H}|_{ijk}^n \end{bmatrix} = \sum_{n'i'j'k'} \begin{bmatrix} \mathbf{G}_{\mathbf{ee}}|_{i-i'j-j'k-k'}^{n-n'} & \mathbf{G}_{\mathbf{eh}}|_{i-i'j-j'k-k'}^{n-n'} \\ \mathbf{G}_{\mathbf{he}}|_{i-i'j-j'k-k'}^{n-n'} & \mathbf{G}_{\mathbf{hh}}|_{i-i'j-j'k-k'}^{n-n'} \end{bmatrix} \begin{bmatrix} \eta\mathbf{J}_{\mathbf{eq}}|_{i'j'k'}^{n'} \\ \mathbf{M}_{\mathbf{eq}}|_{i'j'k'}^{n} \end{bmatrix} \quad (1)$$

where:

$$\mathbf{J}_{\mathbf{eq}}|_{ijk}^n = (s_x s_y s_z)^{-1} c\Delta t\mathbf{J}|_{ijk}^n \quad (2)$$

$$\mathbf{M_{eq}}|_{ijk}^n = (s_x s_y s_z)^{-1} c \Delta t \mathbf{M}|_{ijk}^n \tag{3}$$

where: $s_p = c\Delta t/\Delta p$ is the Courant number, c denotes the speed of light, Δt is the time-step size, Δp is the discretization-step size along the p-direction ($p = x, y, z$) and n is the time index.

The analytic closed-form expression for the $G_{ee,xz}$ component of dyadic DGF takes the following form in infinite free space for the cell (i, j, k) [4]:

$$G_{ee,xz}|_{i+\frac{1}{2}jk}^n = \sum_{m=n_i}^{n-2} \binom{n+m}{2m+2} g_{xz}|_{ijk}^m \tag{4}$$

where:

$$g_{xz}|_{ijk}^m = -(-1)^{m+i+j+k} \sum_{\substack{\alpha+\beta+\gamma=m \\ \alpha \geqslant \alpha_x \beta \geqslant \beta_x \gamma \geqslant \gamma_x}} \binom{m}{\alpha\beta\gamma}$$

$$\times \binom{2\alpha+1}{\alpha+i+1}\binom{2\beta}{\beta+j}\binom{2\gamma+1}{\gamma+k} s_x^{2\alpha+2} s_y^{2\beta+1} s_z^{2\gamma+2} \tag{5}$$

where: $n_i = \alpha_x + \beta_x + \gamma_x$, $\alpha_x = \max(-i-1, i)$, $\beta_x = |j|$, $\gamma_x = \max(-k, k-1)$. Formulas for other components of dyadic DGF are not presented here for the sake of brevity.

Computation of the electromagnetic field outside the FDTD domain requires to generate DGF waveforms corresponding to the equivalent currents measured over the Huygens surfaces. The DGF generation is a part of preprocessing stage or, alternatively, the DGF waveforms can be read from a file on a hard drive. However, size of available memory and runtime still will limit the feasibility of generation of long DGF waveforms [4, 31–33], as well as at the preprocessing stage. If the length of the DGF waveforms is equal to the number of iterations in the FDTD simulation, the presented techniques return the same results as the direct FDTD method (assuming infinite numerical precision of computations). Since the number of FDTD iterations required for the convergence of a simulation is unknown in advance and the DGF generation and convolution computations require processor time, DGF has to be truncated with appropriate windowing function [13]:

$$WG|_{ijk}^n = W^n \cdot G|_{ijk}^n \tag{6}$$

$$W^n = \begin{cases} 0, & n < n_i \\ 1, & n_i \leqslant n < n_0 \\ w^n, & n_0 \leqslant n < n_t \\ 0, & n_t \leqslant n \end{cases} \tag{7}$$

Since the DGF values are nonzero only for $n \geqslant n_i$, the window length is defined as $n_s = n_t - n_i$. The value of n_i coefficient corresponds to the moment of the DGF wavefront arrival in the FDTD grid, refer to (4). The window function consists of a constant range ($W^n = 1$) and a tapering function range ($W^n = w^n$). Such a formula of windowing modifies only a tail of the DGF waveform. The constant range to total window length ratio (CTR) for the considered windowing function was defined as a quotient of the number of samples with $W^n = 1$ and the total window size n_s:

$$\mathrm{CTR} = \frac{n_0 - n_i}{n_s} \qquad (8)$$

Although waves generated on the Huygens box arrive to the observation point at different moments n_i, parameters of the windowing function (w_n, CTR, n_s) are the same for all DGFs on the Huygens box. The Hann's tapering function was employed in the developed implementation [34]:

$$w^n = 0.5 \left[1 + \cos \left(\pi \frac{n - n_0}{n_t - n_0} \right) \right] \qquad (9)$$

The usefulness of the Hann's window in electromagnetic computations has already been demonstrated in [35]. Independently, it was verified that the Hann's window provides the best performance of the DGF truncation [36], comparing to other functions which have already been employed for this purpose in the literature [3, 13].

3. APPLICATION OF CGF INSTEAD OF DGF IN THE FDTD METHOD

Although it may seem at first glance that CGF can be applied instead of DGF in the FDTD method, drawbacks of this approach are demonstrated and discussed here. Only the $\widetilde{G}_{ee,xz}$ component of dyadic CGF is considered for the sake of brevity. Its expression in the infinite free space takes the following form for the cell (i, j, k) and the continuous time $t = n\Delta t$ [4]:

$$\widetilde{G}_{ee,xz}(t = n\Delta t)|_{i+\frac{1}{2}jk} = \frac{\sin \theta_x \cos \theta_x \cos \phi_x}{4\pi} \frac{\eta \Delta x \Delta y \Delta z}{(c\Delta t)^2}$$
$$\times \left\{ \frac{3U[(n - R_x)\Delta t]}{R_x^3 \Delta t} + \frac{3\delta[(n - R_x)\Delta t]}{R_x^2} + \frac{\delta'[(n - R_x)\Delta t]}{R_x} \Delta t \right\} \quad (10)$$

where $U(t)$ is the unit step function, $\delta(t)$ is the Dirac delta function, (θ_x, ϕ_x) are the azimuthal and polar angles for the spherical coordinates of the observation point $((i + 1/2)\Delta x, j\Delta y, k\Delta z)$ with respect to the

source point $(0, 0, 1/2\Delta z)$ (in Cartesian coordinates). R_x denotes the normalized distance:

$$R_x = \sqrt{\left(\frac{i + 1/2}{s_x}\right)^2 + \left(\frac{j}{s_y}\right)^2 + \left(\frac{k - 1/2}{s_z}\right)^2} \qquad (11)$$

The waveform (10) is not bandlimited thus sampling based on the Nyquist theorem cannot be applied in this case [34]. However, the convolution with the unit step function is equivalent to the integration that can be represented as an integrator filter in the discrete-time domain. The convolution with the first-order derivative of the Dirac delta is equivalent to the differentiation that can be represented as a differentiator filter in the discrete-time domain. The Dirac delta is an identity element for the convolution in the continuous-time domain whereas the Kronecker delta is the identity element for the convolution in the discrete-time domain. Therefore, the following equivalences hold between the continuous- and discrete-time domains:

$$\begin{aligned} U(t) &\longrightarrow u|^n \\ \delta(t) &\longrightarrow \delta|^n \\ \delta'(t) &\longrightarrow \delta'|^n \end{aligned} \qquad (12)$$

where $u|^n$ is the discrete-time integrator implemented as the unit step in the discrete domain, $\delta|^n$ the Kronecker delta, and $\delta'|$ the discrete-time differentiator. In the first instance, the differentiator can be implemented as the first-order backward difference:

$$\delta'|^n = \frac{\delta|^n - \delta|^{n-1}}{\Delta t} \qquad (13)$$

In this way, one can obtain the following algorithm of the digital filtration:

$$\begin{aligned} \widetilde{G}_{ee,xz}|^n_{i+\frac{1}{2}jk} &= \frac{\sin\theta_x \cos\theta_x \cos\phi_x}{4\pi} \frac{\eta\Delta x\Delta y\Delta z}{(c\Delta t)^2} \\ &\quad \times \left\{ \frac{3u|^{n-R_x}}{R_x^3\Delta t} + \frac{3\delta|^{n-R_x}}{R_x^2} + \frac{\delta'|^{n-R_x}}{R_x}\Delta t \right\} \end{aligned} \qquad (14)$$

Unfortunately, the obtained formula may not be compatible with the time-marching procedure of the FDTD method because R_x is not an integer in general. For instance, R_x is equal to 64.3545 for the cell $(10, 20, 30)$ and $s_x = s_y = s_z = 1/\sqrt{3}$. The exact representation of the fractional shift $\alpha = R_x - \lfloor R_x \rfloor$ requires execution of the resampling process. The desired solution can be obtained by first reconstructing the continuous bandlimited signal and then resampling

it after shifting [37]:

$$x_\alpha|^n = x[(n + \alpha)\Delta t] = \sum_{k=-\infty}^{+\infty} x|^k \frac{\sin \pi(n - k + \alpha)}{\pi(n - k + \alpha)} \tag{15}$$

Although these computations are equivalent to the linear filtration, the impulse response of such a filter is not only infinite but also noncasual for noninteger α. Fig. 2(a) shows implementation (12)–(14) of CFG for the cell $(10, 20, 30)$. Its filtration (15) with the use
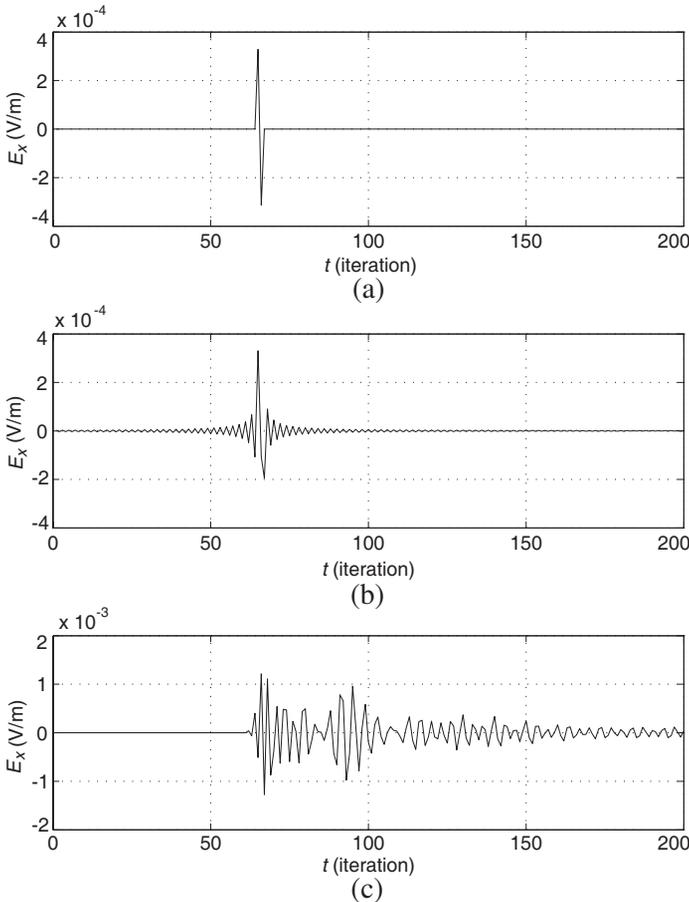

Figure 2. Time-domain waveforms of (a) $\widetilde{G}_{ee,xz}|^n$ component of dyadic CGF, (b) α-shifted $\widetilde{G}_{ee,xz}|^n$ component of dyadic CGF and (c) $G_{ee,xz}|^n$ component of dyadic DGF for the cell $(10, 20, 30)$.

of $\sin\pi(n+\alpha)/(\pi(n+\alpha))$ is shown in Fig. 2(b). As seen, such a representation of CGF in the discrete domain is noncasual since pulses arrive to the observation point before the time $t = cR_x$. On the other hand, although DGF allows superluminal propagation like the FDTD method [38], the DGF waveform is equal to 0 for $n < n_i$ (see Fig. 2(c)).

Any application of fractional delay filters (e.g., based on Lagrange interpolation [37] or B-splines [39, 40]) will involve approximations or noncasual solutions. Low-error approximations converge to the formula of the resampling process (15) which is the only accurate solution in the discrete domain. However, CGF after the filtration (15) may not be casual (i.e., equal to 0 for $n < n_i$), thus its applicability in the FDTD method may lead to physically wrong results. Therefore, DGF is applied in the developed FDTD method on disjoint domains because DGF is casual and compatible with the discrete FDTD domain.

4. NUMERICAL RESULTS

The described above DGF-based techniques were implemented in the developed FDTD solver on disjoint domains. Numerical tests were executed in double floating-point precision. In the presented results of investigations, the methods [31–33] were employed for the DGF generation. The Courant numbers were taken as $s_x = s_y = s_z = 0.99/\sqrt{3}$. The relative error between vector results generated using the evaluated technique $[\mathbf{E}|_{ijk}^n]$ and the reference solution $[\mathbf{E_{ref}}|_{ijk}^n]$ was calculated as:

$$\text{Error} = 20\log_{10}\left[\frac{\max\left|\mathbf{E}|_{ijk}^n - \mathbf{E_{ref}}|_{ijk}^n\right|}{\max\left|\mathbf{E_{ref}}|_{ijk}^n\right|}\right] \text{ (dB)} \qquad (16)$$

Such a formula for error calculation is insensitive to distortions of a single field component which values are negligible in comparison to the maximal length of the field vector.

4.1. Radiated Field Computations

Accuracy of the radiated field computations was evaluated in comparison with the convolution of a current source waveform with DGF. Such a reference solution is equivalent to the FDTD simulation in the infinite Yee's grid, thus reference waveforms are not distorted by reflections from imperfect PMLs. It was verified that the error of the radiated field computations is less than $-130\,\text{dB}$ for the DGF lengths equal to the total number of time steps in a simulation. It proves that

the Huygens box, PMLs, DGFs and the convolution computations were correctly implemented in the software.

Figure 3 shows accuracy of the DGF implementation of the radiated field computations against the length of windowing function for varied position of the observation point (i, j, k). Results for the ramped sinusoid (with frequency corresponding to the wavelength
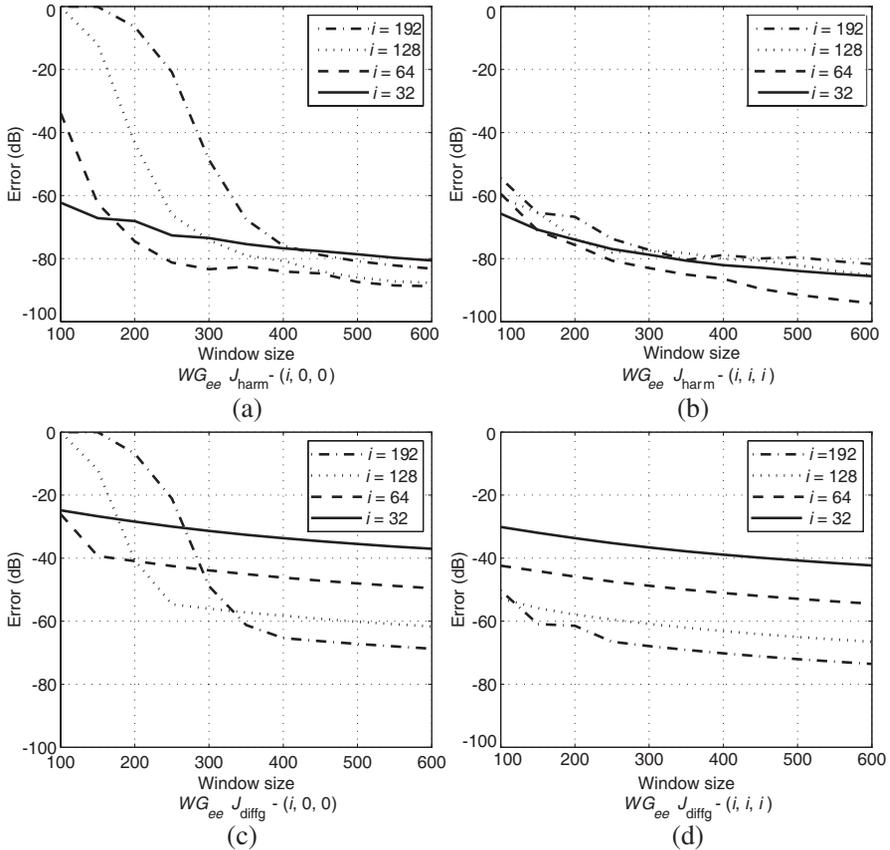

Figure 3. Error of the electric field vectors computed using the windowed DGF propagators vs. window length. (a) and (b) Ramped harmonic current source excited the center of the Huygens box with the corresponding wavelength equal to $20\Delta x$. (c) and (d) Differentiated Gaussian pulse excited the center of the Huygens box with the maximal frequency in the spectrum corresponding to the wavelength equal to $20\Delta x$. Positions of the observation cell varied in the (a) and (c) axial, and (b) and (d) diagonal directions from the source.

$\lambda = 20\Delta x$) and the differentiated Gaussian (with maximal frequency in the spectrum corresponding to $\lambda = 20\Delta x$) excitations are respectively presented in Figs. 3(a) and (b) and Figs. 3(c) and (d). The CTR parameter was set to 0.5 in both cases, the number of samples was set to 1600 for the source- and the observation-point waveforms. J_z current source was placed in the center of the cubic Huygens box consisting of 27 cells. As seen in Figs. 3(a) and (c), the computations of the radiated field require window length longer than minimal value providing an acceptable error level, e.g., 200 samples for the error below -40 dB and $i = 128$ in the axial direction from source. The convolution of the harmonic excitation lasting 1600 samples with the significantly shorter windowed DGFs resulted in the error below -60 dB for the diagonal direction in the grid, refer to Fig. 3(b). The error is slightly larger for observation points in the axial direction than for the diagonal direction in the grid. For pulse excitation (refer to Figs. 3(c) and (d)), the error in the axial direction is increased for small distance from the source ($i = 32$). In this case, distortions such as small spurious peaks appear in computed waveforms for insufficiently long windowed DGFs.

Figure 4 shows accuracy of the DGF implementation of the radiated field computations vs. CTR value for the excitations as in Figs. 3(a) and (b) and Figs. 3(c) and (d), respectively. The window length was set to 400 samples. Other parameters are the same as in the previous test. As seen, the CTR = 0.5 provides the satisfactory accuracy of the DGF windowing in a wide range of distances from the source and excitation waveforms. Therefore, this CTR value is recommended for windowing of the DGF waveforms. CTR = 1 is equivalent to the case of the DGF truncation using the rectangular window. As seen, such a truncation provides the lowest accuracy of computations.

Figure 5 shows the accuracy of the radiated field computations for varied volume of the Huygens box around the half-wavelength dipole antenna. In this test, the direct FDTD simulation was employed as the reference solution. The DGF window length was set to $n_s = 100$ samples. The observation point was placed in the diagonal direction from the source. As seen, the accuracy of the developed technique (-50 dB) does not change significantly for varied volume of the Huygens box.

4.2. FDTD Simulations on Disjoint Domains with Unilateral Coupling

Figure 6 shows the accuracy of computations when the radiated field excites a coupled TFSF domain (both FDTD domains of size 26^3 cells, terminated by 10 PMLs). J_z source was placed in the center of the
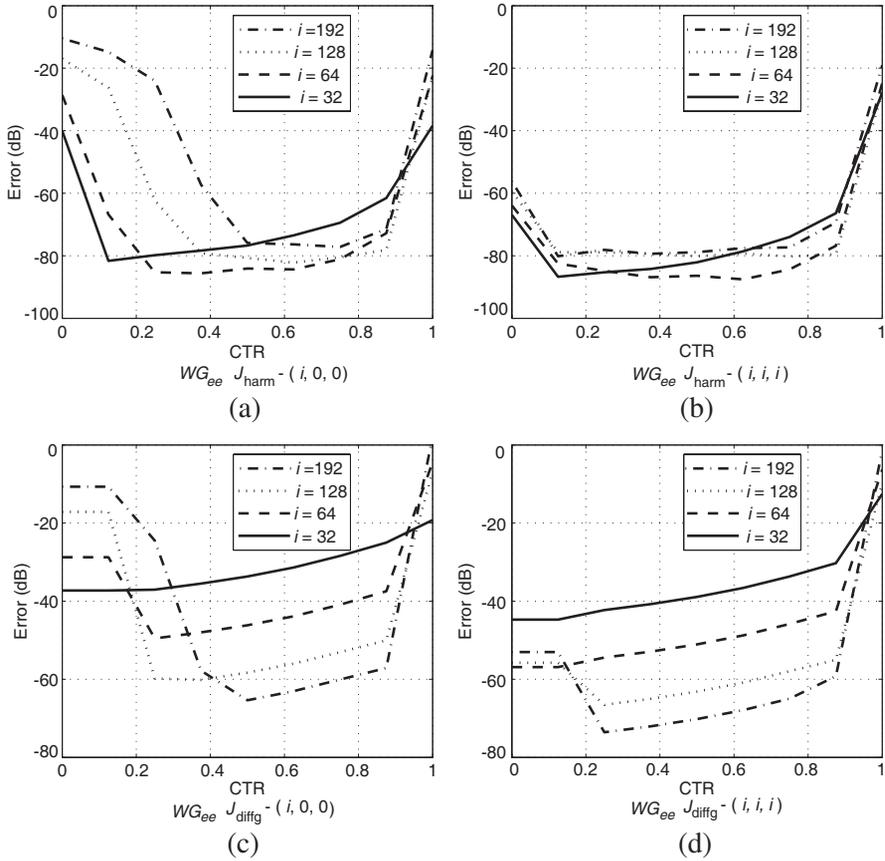
Figure 4. Error of the electric field vectors computed using the windowed DGF propagators vs. CTR parameter value. (a) and (b) Ramped harmonic current source excited the center of the Huygens box with the corresponding wavelength equal to $20\Delta x$. (c) and (d) Differentiated Gaussian pulse excited the center of the Huygens box with the maximal frequency in the spectrum corresponding to the wavelength equal to $20\Delta x$. Positions of the observation cell varied in the (a) and (c) axial, and (b) and (d) diagonal directions from the source.

radiating domain whereas observation point was in the center of the coupled TFSF domain. The error is between -75 dB and -60 dB for varying position of the domain with the observation point. It was noticed that errors are higher for wideband excitations with spectrum starting from low frequency contents (e.g., differentiated Gaussian
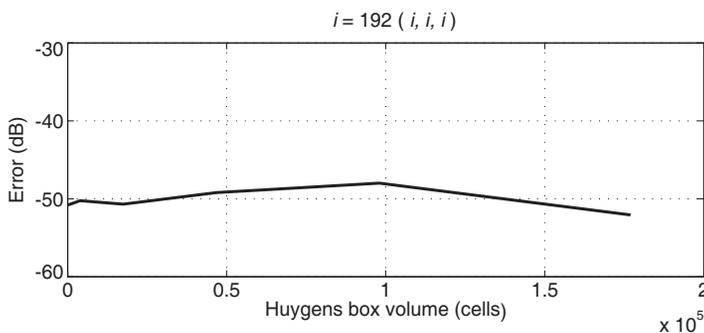
Figure 5. Maximum relative error between the electric field vectors computed using the windowed DGF propagators and the FDTD method vs. volume of the Huygens box around the antenna. The half-wavelength dipole radiating inside the center of the Huygens box was excited by ramped sinusoid ($\lambda = 20\Delta x$).
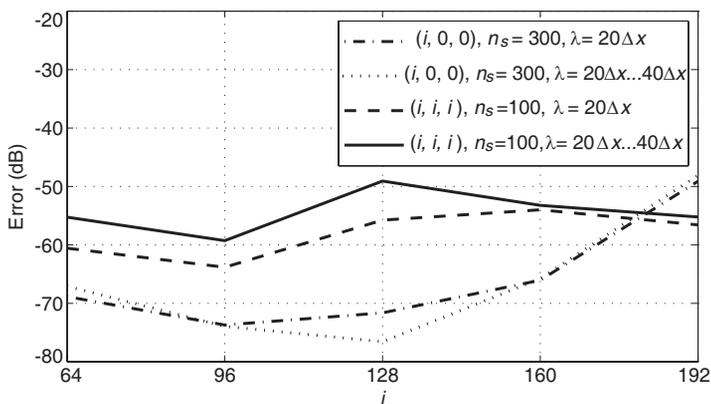

Figure 6. Error of the electric field vectors in the TFSF domain excited by the radiated field (computed using windowed DGF propagators) vs. position of the observation cell from the source. Ramped sinusoid ($\lambda = 20\Delta x$) and Gaussian modulated ($\lambda/\Delta x = 20 - 40$) current sources excited the Huygens box of size 64 cells. The coupled total-field domain was of size 64 cells as well.

source). Therefore, the modulated Gaussian source, with the frequency band corresponding to the wavelengths $20\Delta x$ and $40\Delta x$, was employed in this test.

4.3. FDTD Simulations on Disjoint Domains with Bilateral Coupling

Two half-wavelength ($\lambda = 20\Delta x$) dipoles were placed inside the bilaterally coupled FDTD domains, each with the Huygens box of size $4 \times 4 \times 15$ cells. The modulated Gaussian current source (the corresponding wavelengths $\lambda/\Delta x = 16 - 26.6$) excited the transmitting antenna whereas the electric field was measured by the receiving antenna in the coupled domain. The relative position of both domains was varied in the direction $(i, i, 0)$, where $i = 8, 16, 32, 64, 128$. Exemplary waveforms, compared with the result of the direct FDTD simulation, are presented in Fig. 7. As seen, waveforms computed using both methods overlap. The differences between waveforms obtained using the FDTD method on disjoint domains and the direct FDTD method are presented in Fig. 8. As seen, the error of the field measured by the receiving antenna is around 20 dB higher than measured in the source. It stems from a relatively weak coupling between the antennas and stronger influence of the DGF truncation on the coupled domain. For $i \geqslant 16$, the error measured in the source is almost constant because the impact of the receiving antenna on the source is relatively low in this case.
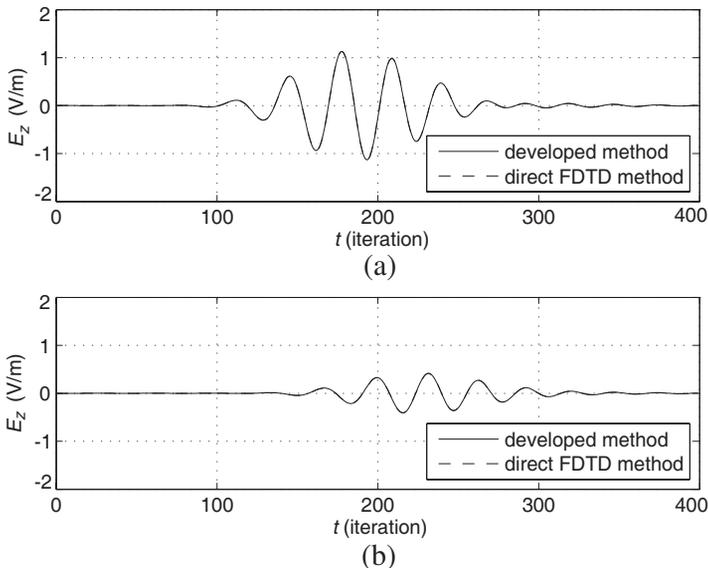

Figure 7. Exemplary waveforms measured by (a) the transmitting antenna and (b) the receiving antenna (shift between antennas: $(i, i, 0) = (8, 8, 0)$, modulated Gaussian excitation ($\lambda/\Delta x = 16 - 26.6$), Hann's window length $n_s = 100$).
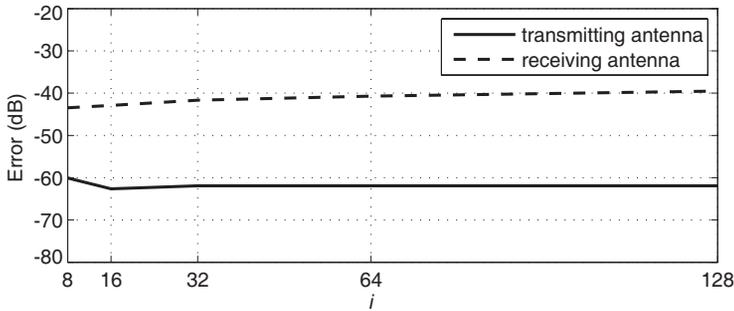
Figure 8. Error of the electric field measured by the transmitting antenna and the receiving antenna in the bilaterally coupled FDTD domains vs. shift between domains (modulated Gaussian excitation with $\lambda/\Delta x = 16 - 26.6$, Hann's window length $n_s = 100$).

4.4. Summary and Discussion of Numerical Results

The runtime scaling of the DGF convolution computations executed over M cells at the Huygens box is of order (Mn_s) for a single observation point. Therefore, the runtime scaling is of order $(M^2 n_s)$ for two coupled domains (computational cost of FDTD updates is neglected). On the other hand, the direct FDTD computations require updating of all cells in the extended domain including coupled subdomains and all observation points in the far-field zone. The runtime scaling of these computations is of order (N^3), where N^3 denotes the number of cells in a cubic domain. Therefore, efficiency of the FDTD method on disjoint domains is higher than the direct FDTD method if small domains are simulated and distance between them is sufficiently long $(M^2 n_s \ll N^3)$.

The length of DGF waveforms equal to the number of iterations in an FDTD simulation guarantees that the presented techniques return the same results as the direct FDTD method (assuming infinite numerical precision of computations). However, the DGF generation represents the rate limiting step of the proposed computational techniques. Although the DGF generation can be significantly accelerated with the use of parallel processing [31–33], size of available memory and runtime currently limit the feasibility of generation of long DGF waveforms. Therefore, in the presented results of computations, DGF waveforms are truncated to speed up computations and the windowing technique is applied to increase the accuracy of results. Currently, the DGF applicability faces the tradeoff between accuracy and runtime. Therefore, the presented DGF techniques are of limited

practical use. However, it can be anticipated that the development of new fast methods of the DGF generation in the future will improve applicability of these techniques in FDTD simulations.

The developed 3-D FDTD method on disjoint domains holds many applications for future work. For instance, simultaneous simulations of a transmitter and a receiver in radio communication systems are possible with the use of this method. The FDTD method on disjoint domains is also open for further extensions including multiple-domain FDTD simulations with many sources and scatterers placed in separate subdomains. Moreover, DGF allows to decompose the FDTD domain in order to execute computations on distributed memory parallel architectures with subdomains updated by different processing units.

5. CONCLUSIONS

The FDTD method on disjoint domains and computations of the electromagnetic field radiated by the FDTD domain are the DGF applications examined in this paper. DGF is directly derived from the FDTD update equations, thus the FDTD method and its integral discrete formulation based on DGF can be perfectly coupled. Unfortunately, the DGF generation requires significant processor time. Therefore, the infinite DGF waveforms are truncated using the Hann's window and accuracy of this approximation has been demonstrated. Currently, the DGF applicability faces the tradeoff between accuracy and runtime. It can be anticipated that the development of new fast methods of the DGF generation in the future will improve applicability of these techniques in FDTD simulations.

REFERENCES

1. Vazquez, J. and C. G. Parini, "Discrete Green's function formulation of FDTD method for electromagnetic modelling," *Electron. Lett.*, Vol. 35, No. 7, 554–555, 1999.
2. Holtzman, R. and R. Kastner, "The time-domain discrete Green's function method (GFM) characterizing the FDTD grid boundary," *IEEE Trans. Antennas Propag.*, Vol. 49, No. 7, 1079–1093, 2001.

3. Holtzman, R, R. Kastner, E. Heyman, and R. W. Ziolkowski, "Stability analysis of the Green's function method (GFM) used as an ABC for arbitrarily shaped boundaries," *IEEE Trans. Antennas Propag.*, Vol. 50, No. 7, 1017–1029, 2002.

4. Jeng, S.-K., "An analytical expression for 3-D dyadic FDTD-compatible Green's function in infinite free space via z-transform and partial difference operators," *IEEE Trans. Antennas Propag.*, Vol. 59, No. 4, 1347–1355, 2011.

5. Taflove, A. and S. C. Hagness, *Computational Electrodynamics: The Finite-difference Time-domain Method*, 3rd edition, Artech House, Boston, 2005.

6. Xiao, S.-Q., Z. Shao, and B.-Z. Wang, "Application of the improved matrix type FDTD method for active antenna analysis," *Progress In Electromagnetics Research*, Vol. 100, 245–263, 2010.

7. Lee, K. H., I. Ahmed, R. S. M. Goh, E. H. Khoo, E. P. Li, and T. G. G. Hung, "Implementation of the FDTD method based on Lorentz-Drude dispersive model on GPU for plasmonics applications," *Progress In Electromagnetics Research*, Vol. 116, 441–456, 2011.

8. Kong, L.-Y., J. Wang, and W.-Y. Yin, "A novel dielectric conformal FDTD method for computing SAR distribution of the human body in a metallic cabin illuminated by an intentional electromagnetic pulse (IEMP)," *Progress In Electromagnetics Research*, Vol. 126, 355–373, 2012.

9. Xiong, R., B. Chen, J.-J. Han, Y.-Y. Qiu, W. Yang, and Q. Ning, "Transient resistance analysis of large grounding systems using the FDTD method," *Progress In Electromagnetics Research*, Vol. 132, 159–175, 2012.

10. Noroozi, Z. and F. Hojjat-Kashani, "Three-dimensional FDTD analysis of the dual-band implantable antenna for continuous glucose monitoring," *Progress In Electromagnetics Research Letters*, Vol. 28, 9–21, 2012.

11. Wahl, P., D. S. Ly Gagnon, C. Debaes, J. Van Erps, N. Vermeulen, D. A. B. Miller, and H. Thienpont, "B-calm: An open-source multi-gpu-based 3D-FDTD with multi-pole dispersion for plasmonics," *Progress In Electromagnetics Research*, Vol. 138, 467–478, 2013.

12. Ma, W., M. R. Rayner, and C. G. Parini, "Discrete Green's function formulation of the FDTD method and its application in antenna modeling," *IEEE Trans. Antennas Propag.*, Vol. 53, No. 1, 339–346, 2005.

13. Vazquez, J. and C. G. Parini, "Antenna modelling using discrete

Green's function formulation of FDTD method," *Electron. Lett.*, Vol. 35, No. 13, 1033–1034, 1999.

14. Holtzman, R., R. Kastner, E. Heyman, and R. W. Ziolkowski, "Ultra-wideband cylindrical antenna design using the Green's function method (GFM) as an absorbing boundary condition (ABC) and the radiated field propagator in a genetic optimization," *Microw. Opt. Tech. Lett.*, Vol. 48, No. 2, 348–354, 2006.

15. Mirhadi, S., M. Soleimani, and A. Abdolali, "An FFT-based approach in acceleration of discrete Green's function method for antenna analysis," *Progress In Electromagnetics Research M*, Vol. 29, 17–28, 2013.

16. Tan, T. and M. Potter, "Optimized analytic field propagator (O-AFP) for plane wave injection in FDTD simulations," *IEEE Trans. Antennas Propag.*, Vol. 58, No. 3, 824–831, 2010.

17. Merewether, D. E. and R. Fisher, "An application of the equivalence principle to the finite-difference analysis of EM fields inside complex cavities driven by large apertures," *Proc. IEEE Antennas Propag. Soc. Int. Symp.*, 495–498, 1982.

18. Schneider, J. B. and K. Abdijalilov, "Analytic field propagation TFSF boundary for FDTD problems involving planar interfaces: PECs, TE, and TM," *IEEE Trans. Antennas Propag.*, Vol. 54, No. 9, 2531–2542, 2006.

19. Chew, W. C., "Electromagnetic theory on a lattice," *Journal of Applied Physics*, Vol. 75, No. 10, 4843–4850, 1994.

20. Clemens, M. and T. Weiland, "Discrete electromagnetism with the finite integration technique," *Progress In Electromagnetics Research*, Vol. 32, 65–87, 2001.

21. Schuhmann, R. and T. Weiland, "Conservation of discrete energy and related laws in the finite integration technique," *Progress In Electromagnetics Research*, Vol. 32, 301–316, 2001.

22. Bossavit, A., "'Generalized finite differences' in computational electromagnetics," *Progress In Electromagnetics Research*, Vol. 32, 45–64, 2001.

23. Teixeira, F. L., "Geometric aspects of the simplicial discretization of Maxwell's equations," *Progress In Electromagnetics Research*, Vol. 32, 171–188, 2001.

24. Mouysset, V. P., A. Mazet, and P. Borderies, "Efficient treatment of 3D time-domain electromagnetic scattering scenes by disjointing sub-domains and with consistent approximations," *Progress In Electromagnetics Research*, Vol. 71, 41–57, 2007.

25. De Hon, B. P. and J. M. Arnold, "Stable FDTD on disjoint

domains — A discrete Green's function diakoptics approach," *Proc. The 2nd European Conf. on Antennas and Propag. (EuCAP)*, 1–6, 2007.

26. Murbach, M., E. Cabot, E. Neufeld, M.-C. Gosselin, A. Christ, K. P. Pruessmann, and N. Kuster, "Local SAR enhancements in anatomically correct children and adult models as a function of position within 1.5 T MR body coil," *Progress in Biophysics and Molecular Biology*, Vol. 107, No. 3, 428–433, 2011.

27. Benkler, S., N. Chavannes, and N. Kuster, "Novel FDTD Huygens source enables highly complex simulation scenarios on ordinary PCs," *Proc. IEEE Antennas Propag. Soc. Int. Symp.*, 1–4, 2009.

28. Stefanski, T. P., "Discrete Green's function approach to disjoint domain simulations in 3D FDTD method," *Electron. Lett.*, Vol. 49, No. 9, 597–599, 2013.

29. Merewether, D. E., R. Fisher, and F. W. Smith, "On implementing a numeric Huygen's source scheme in a finite difference program to illuminate scattering bodies," *IEEE Trans. Nucl. Sci.*, Vol. 27, No. 6, 1829–1833, 1980.

30. Martin, T., "An improved near- to far-zone transformation for the finite-difference time-domain method," *IEEE Trans. Antennas Propag.*, Vol. 46, No. 9, 1263–1271, 1998.

31. Stefanski, T. P., "Fast implementation of the FDTD-compatible Green's function on multicore processor," *IEEE Antennas Wireless Propag. Lett.*, Vol. 11, 81–84, 2012.

32. Stefanski, T. P. and K. Krzyzanowska, "Implementation of FDTD-compatible Green's function on graphics processing unit," *IEEE Antennas Wireless Propag. Lett.*, Vol. 11, 1422–1425, 2012.

33. Stefanski, T. P., "Implementation of FDTD-compatible Green's function on heterogeneous CPU-GPU parallel processing system," *Progress In Electromagnetics Research*, Vol. 135, 297–316, 2013.

34. Oppenheim, A. V., R. W. Schafer, and J. R. Buck, *Discrete-time Signal Processing*, 2nd edition, Prentice-Hall, Englewood Cliffs, 1999.

35. Lei, J.-Z., C.-H. Liang, and Y. Zhang, "Study on shielding effectiveness of metallic cavities with apertures by combining parallel FDTD method with windowing technique," *Progress In Electromagnetics Research*, Vol. 74, 85–112, 2007.

36. Stefanski, T. P., "Accuracy of the discrete Green's function formulation of the FDTD method," *IEEE Trans. Antennas Propag.*, Vol. 61, 829–835, 2013.

37. Laakso, T. I., V. Valimaki, M. Karjalainen, and U. K. Laine,

"Splitting the unit delay," *IEEE Signal Proc. Mag.*, Vol. 13, No. 1, 30–60, 1996.

38. Schneider, J. B. and C. L. Wagner, "FDTD dispersion revisited: Faster-than-light propagation," *IEEE Microwave and Guided Wave Lett.*, Vol. 9, No. 2, 54–56, 1999.

39. Olkkonen, J. T. and H. Olkkonen, "Fractional delay filter based on the B-spline transform," *IEEE Signal Proc. Lett.*, Vol. 14, No. 2, 97–100, 2007.

40. Olkkonen, J. T. and H. Olkkonen, "Fractional time-shift B-spline filter," *IEEE Signal Proc. Lett.*, Vol. 14, No. 10, 688–691, 2007.